

Supporting Information for:

**Molecular Dynamics Simulation of the Oil Sequestration
Properties of a Nonionic Rhamnolipid**

Charles M. Luft, Elango Munusamy, Jeanne E. Pemberton, and Steven D. Schwartz*

*Department of Chemistry and Biochemistry, University of Arizona, 1306 East University Blvd.,
Tucson, AZ 85721*

E-mail: sschwartz@email.arizona.edu

Phone: (520) 621-6363

Hydrogen Bonding Interactions

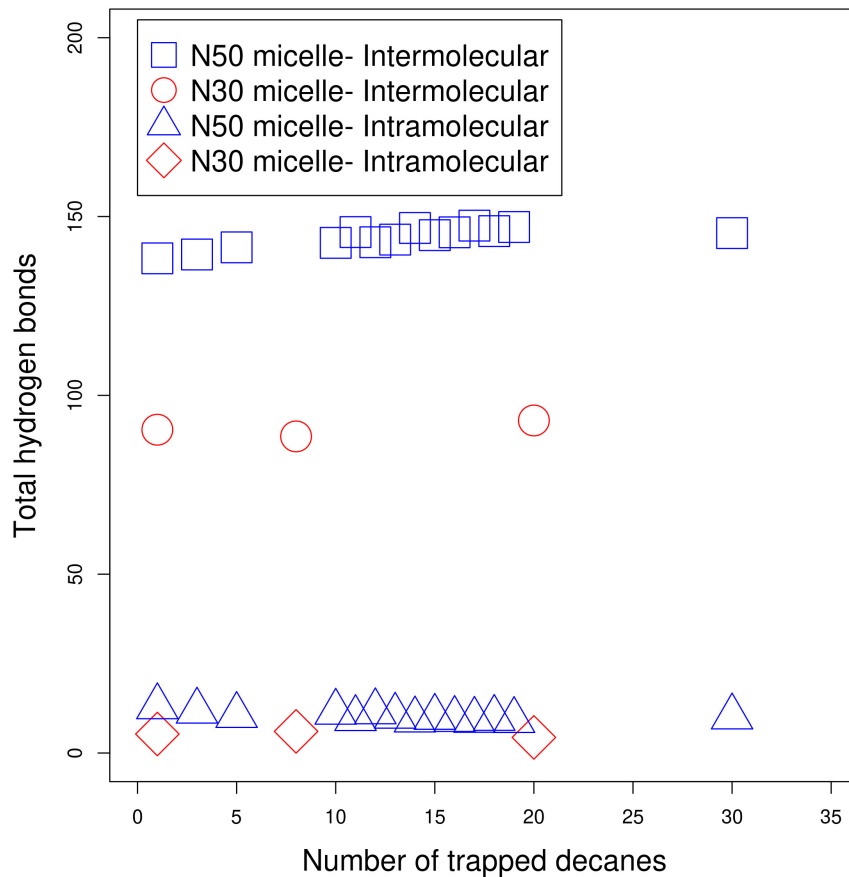
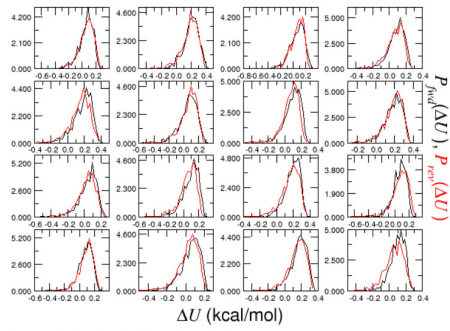


Figure S1. Graph of the number of hydrogen bonds as a function of number of trapped decane molecules. All values are averaged over 5 ns trajectory, 500 data frames each.

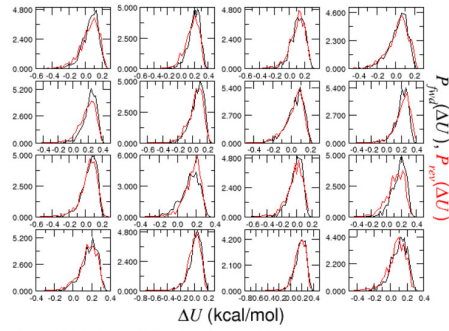
Free Energy Calculations

Figures S2-S9 present the probability distributions for the reversible annihilation as well as the free energy change of trapped decane from micellar systems.

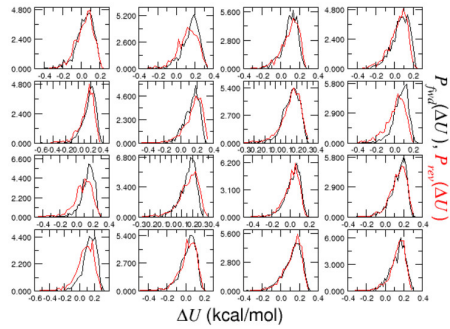
ParseFEP: Probability distribution sheet 1



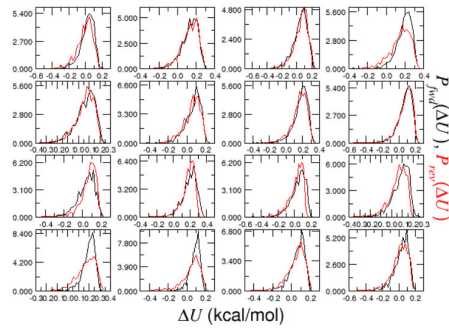
ParseFEP: Probability distribution sheet 2



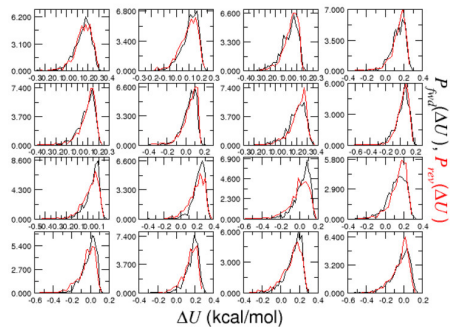
ParseFEP: Probability distribution sheet 3



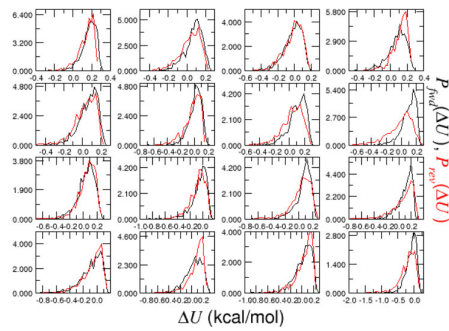
ParseFEP: Probability distribution sheet 4



ParseFEP: Probability distribution sheet 5



ParseFEP: Probability distribution sheet 6



ParseFEP: Probability distribution sheet 7

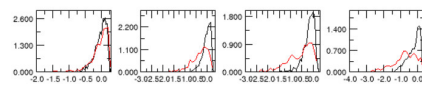
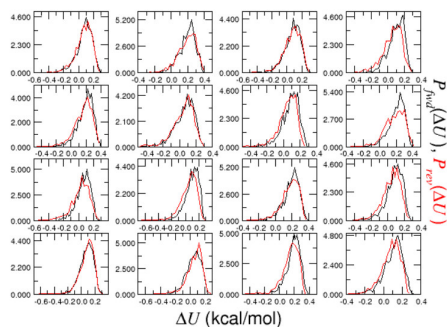
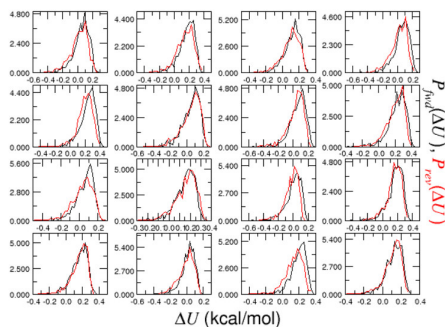


Figure S2. Free energy calculation for N30(D1).

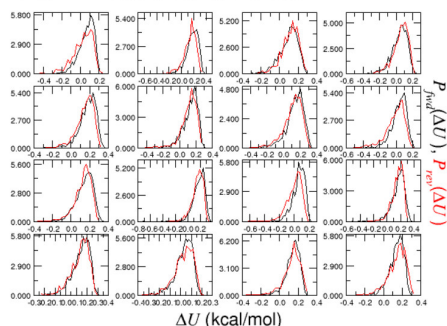
ParseFEP: Probability distribution sheet 1



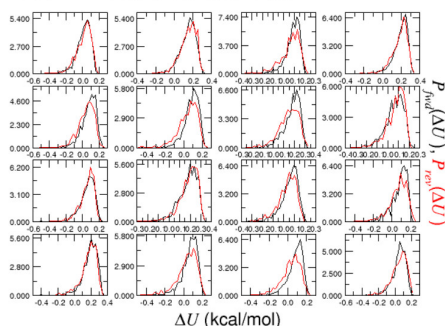
ParseFEP: Probability distribution sheet 2



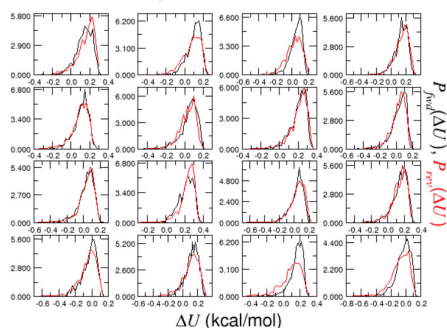
ParseFEP: Probability distribution sheet 3



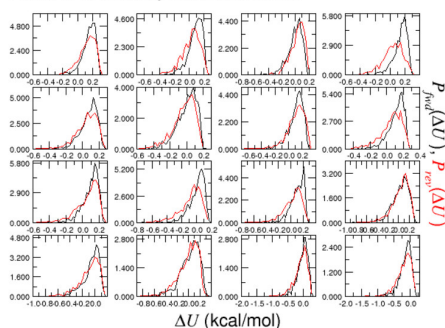
ParseFEP: Probability distribution sheet 4



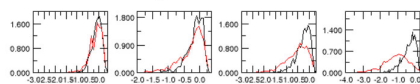
ParseFEP: Probability distribution sheet 5



ParseFEP: Probability distribution sheet 6



ParseFEP: Probability distribution sheet 7



ParseFEP: Summary

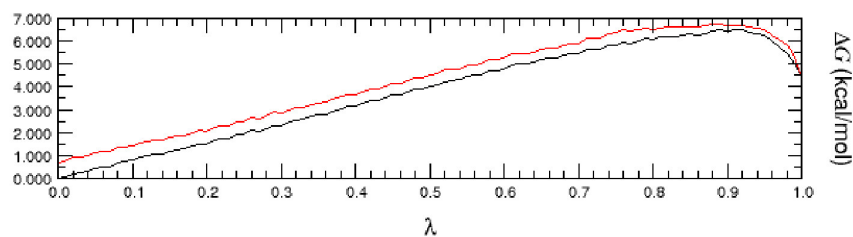
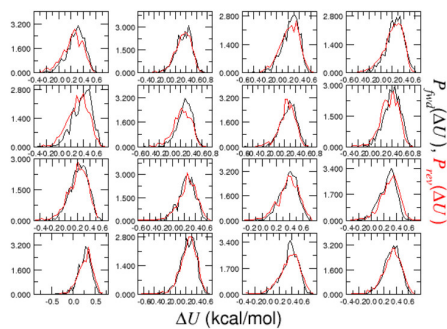
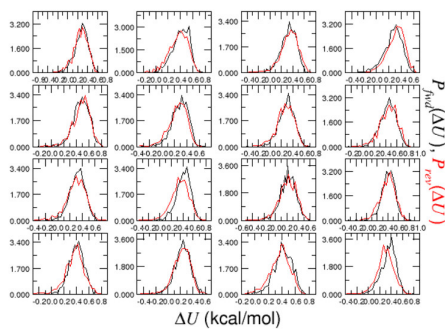


Figure S3. Free energy calculation for N30(D8).

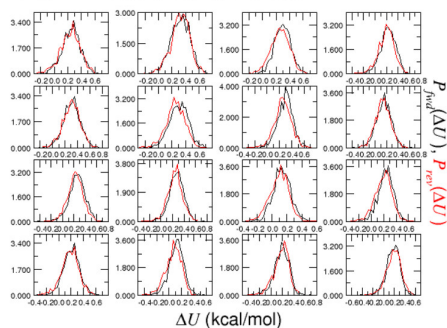
ParseFEP: Probability distribution sheet 1



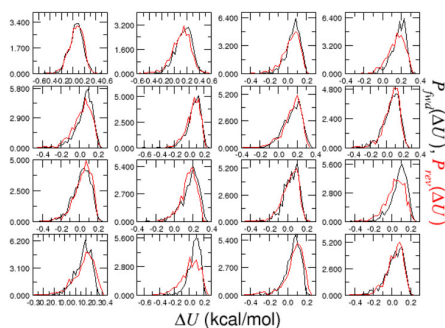
ParseFEP: Probability distribution sheet 2



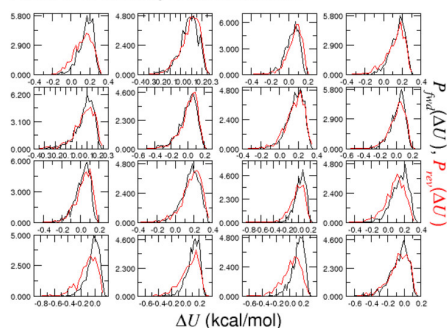
ParseFEP: Probability distribution sheet 3



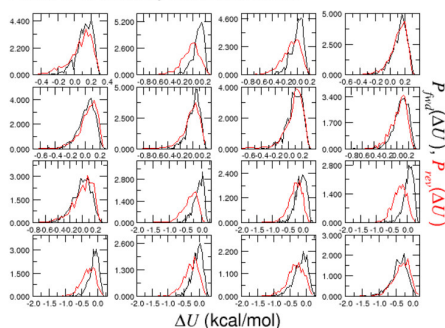
ParseFEP: Probability distribution sheet 4



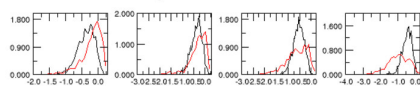
ParseFEP: Probability distribution sheet 5



ParseFEP: Probability distribution sheet 6



ParseFEP: Probability distribution sheet 7



ParseFEP: Summary

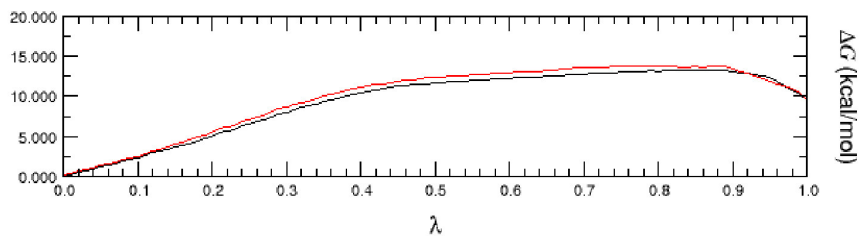
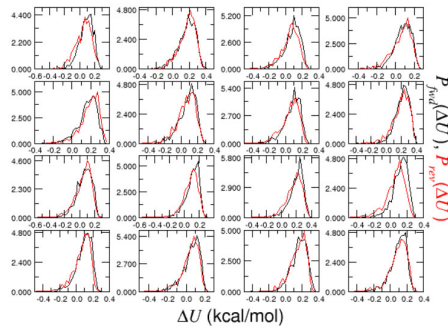
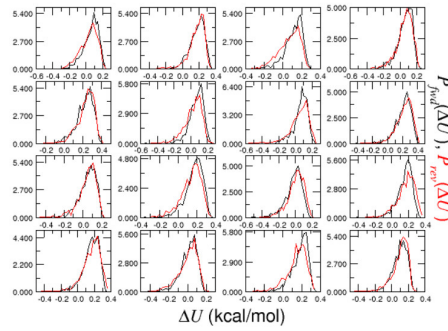


Figure S4. Free energy calculation for N50(D1).

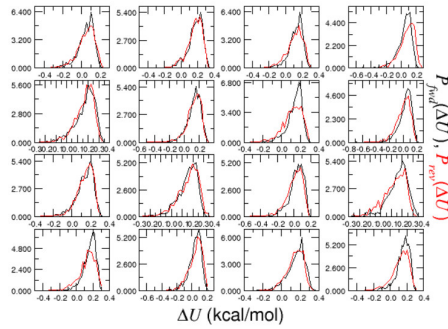
ParseFEP: Probability distribution sheet 1



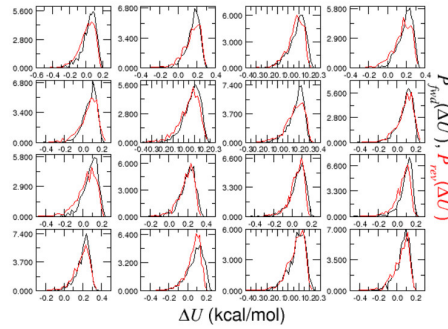
ParseFEP: Probability distribution sheet 2



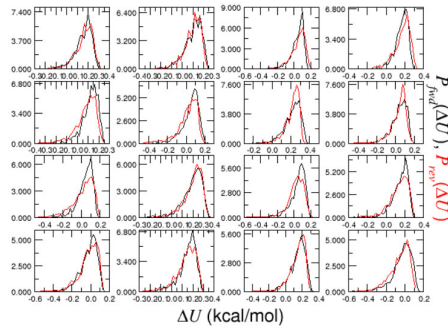
ParseFEP: Probability distribution sheet 3



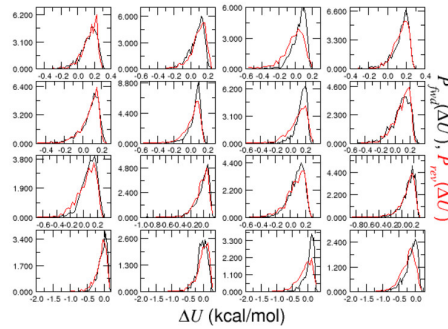
ParseFEP: Probability distribution sheet 4



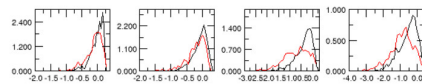
ParseFEP: Probability distribution sheet 5



ParseFEP: Probability distribution sheet 6



ParseFEP: Probability distribution sheet 7



ParseFEP: Summary

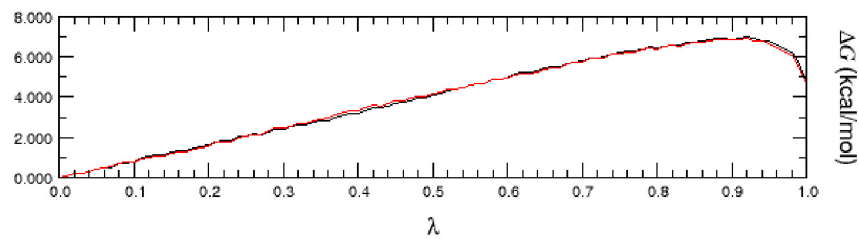
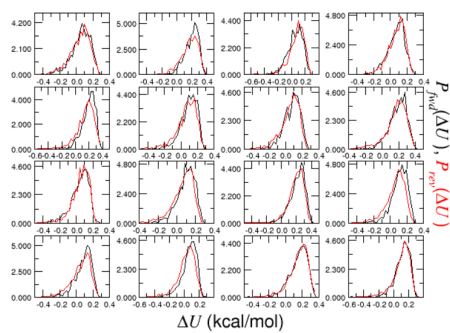
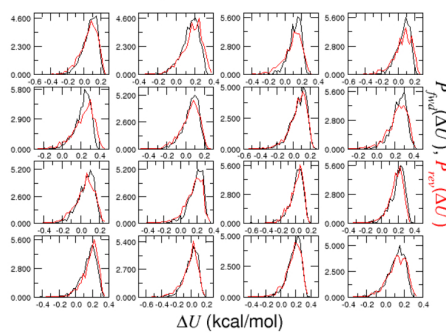


Figure S5. Free energy calculation for N50(D11).

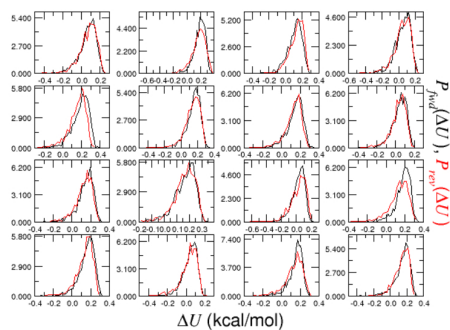
ParseFEP: Probability distribution sheet 1



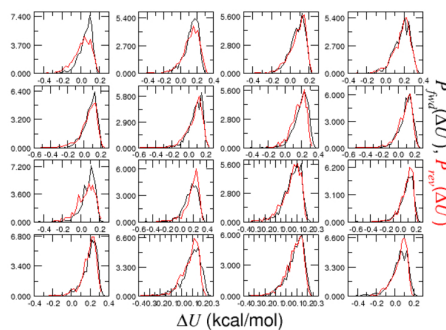
ParseFEP: Probability distribution sheet 2



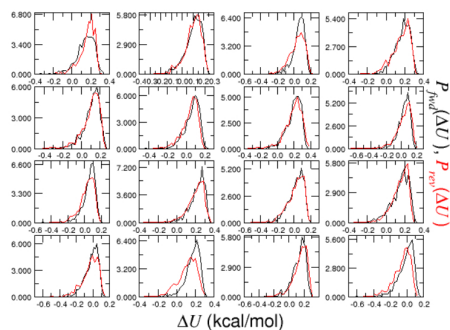
ParseFEP: Probability distribution sheet 3



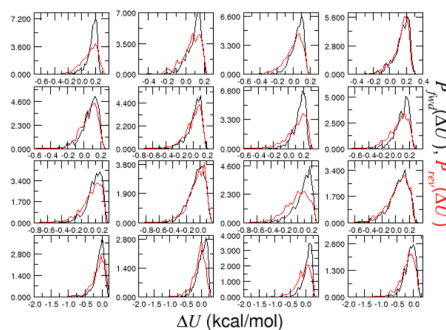
ParseFEP: Probability distribution sheet 4



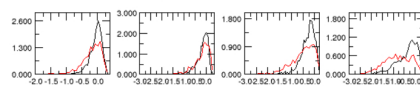
ParseFEP: Probability distribution sheet 5



ParseFEP: Probability distribution sheet 6



ParseFEP: Probability distribution sheet 7



ParseFEP: Summary

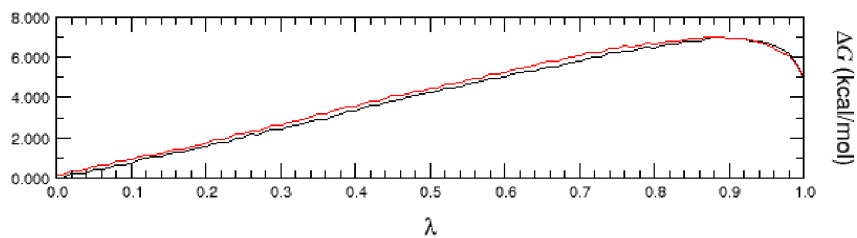
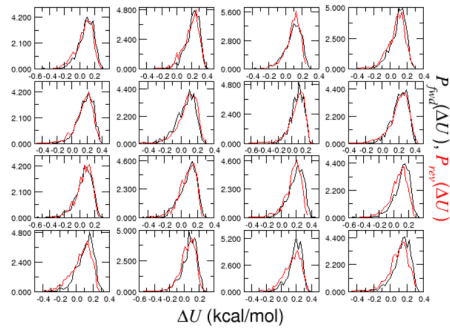
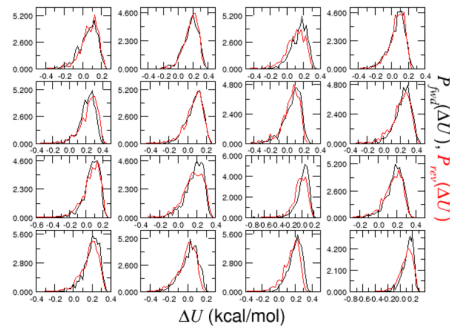


Figure S6. Free energy calculation for N50(D13).

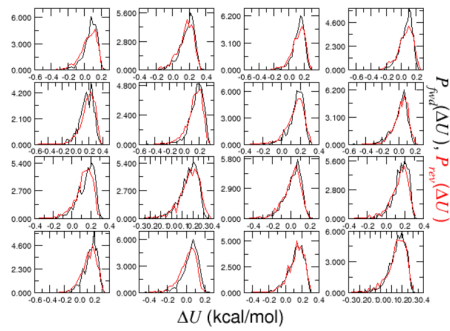
ParseFEP: Probability distribution sheet 1



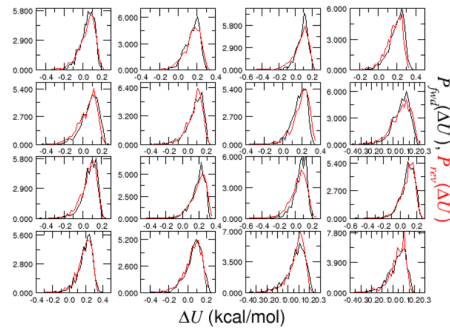
ParseFEP: Probability distribution sheet 2



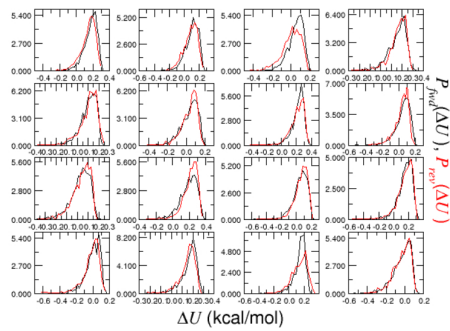
ParseFEP: Probability distribution sheet 3



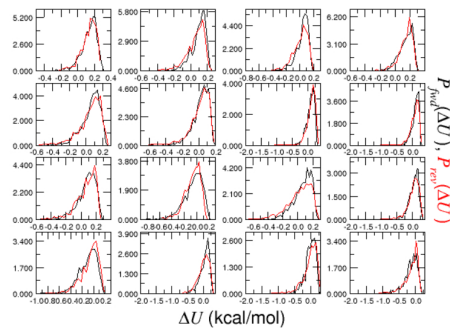
ParseFEP: Probability distribution sheet 4



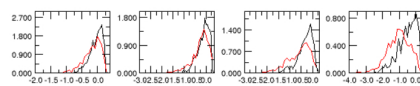
ParseFEP: Probability distribution sheet 5



ParseFEP: Probability distribution sheet 6



ParseFEP: Probability distribution sheet 7



ParseFEP: Summary

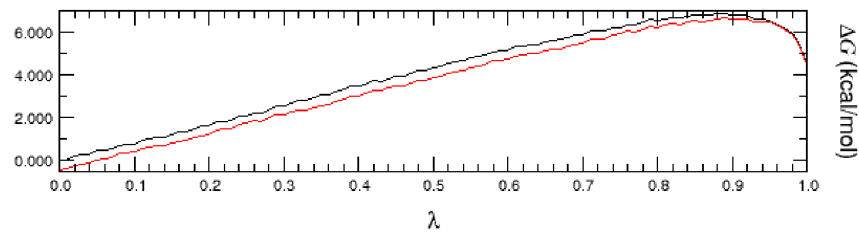
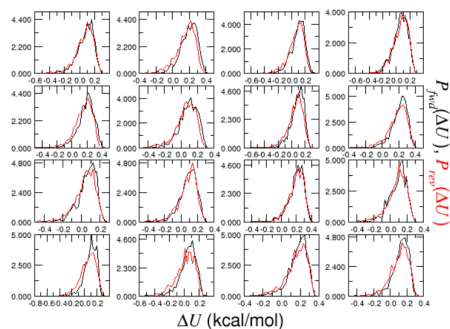
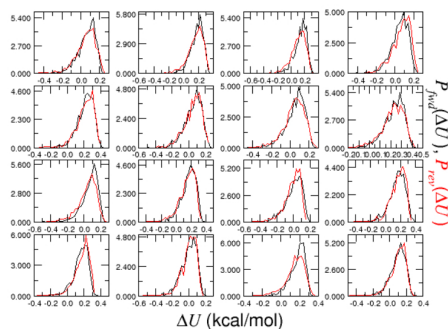


Figure S7. Free energy calculation for N50(D15).

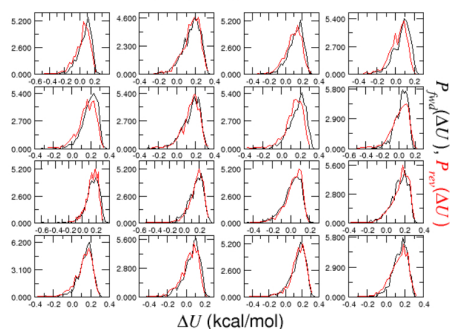
ParseFEP: Probability distribution sheet 1



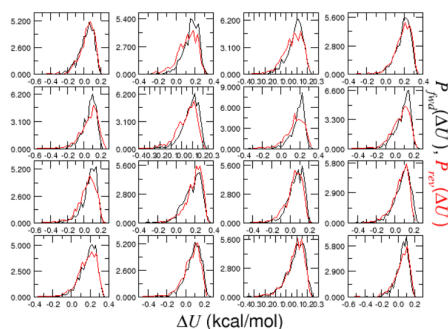
ParseFEP: Probability distribution sheet 2



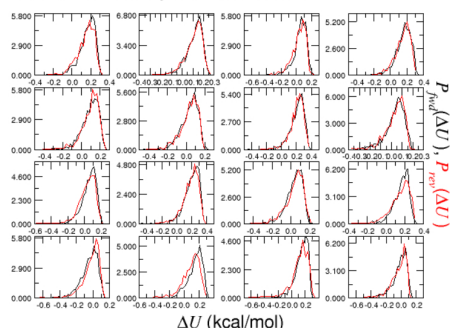
ParseFEP: Probability distribution sheet 3



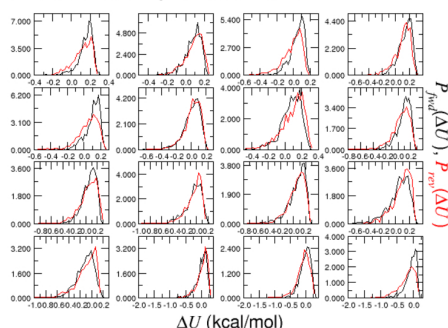
ParseFEP: Probability distribution sheet 4



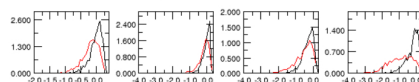
ParseFEP: Probability distribution sheet 5



ParseFEP: Probability distribution sheet 6



ParseFEP: Probability distribution sheet 7



ParseFEP: Summary

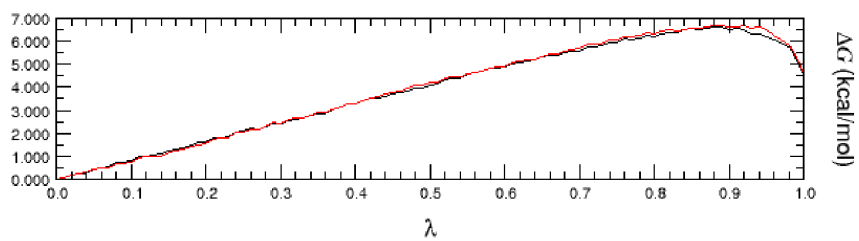
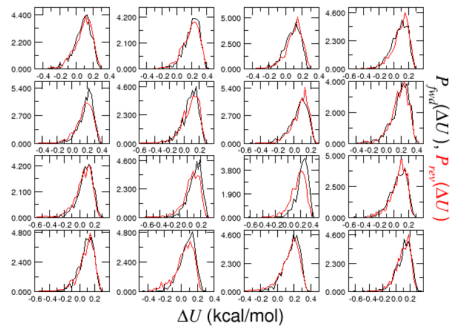
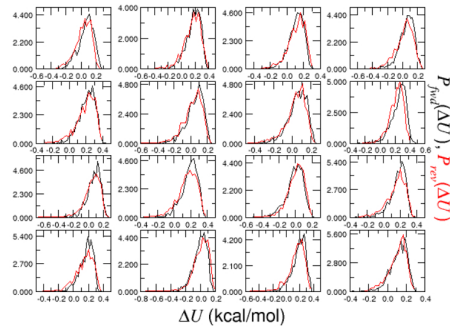


Figure S8. Free energy calculation for N50(D17).

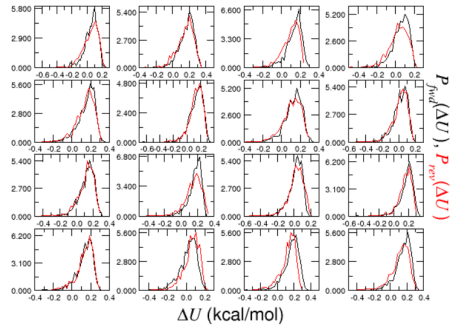
ParseFEP: Probability distribution sheet 1



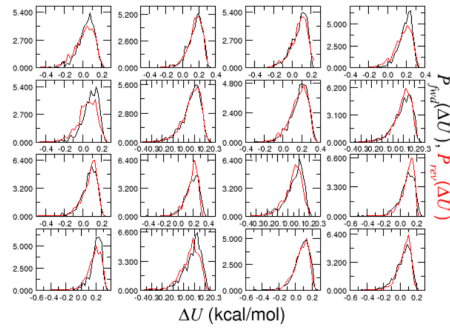
ParseFEP: Probability distribution sheet 2



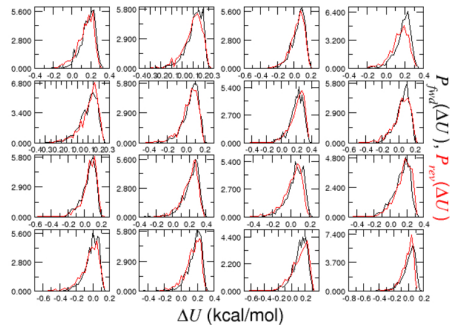
ParseFEP: Probability distribution sheet 3



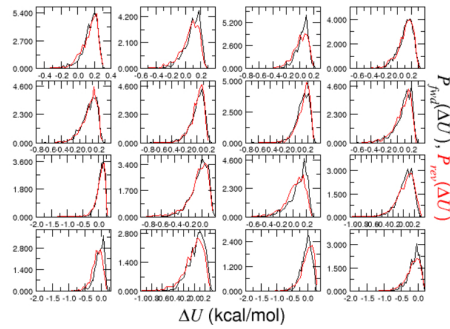
ParseFEP: Probability distribution sheet 4



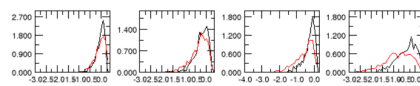
ParseFEP: Probability distribution sheet 5



ParseFEP: Probability distribution sheet 6



ParseFEP: Probability distribution sheet 7



ParseFEP: Summary

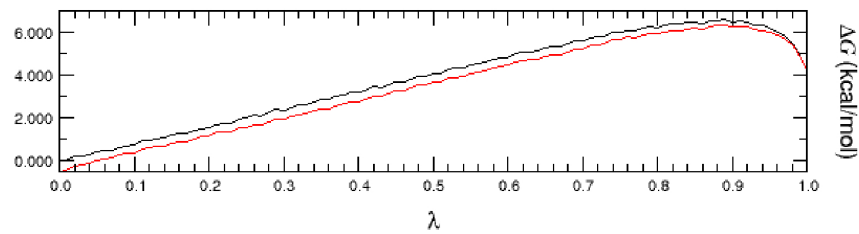


Figure S9. Free energy calculation for N50(D19).

Appendix

Insight into the relative size and shape of the aggregates was obtained from the radius of gyration.

By constructing the radius of gyration tensor for each aggregate defined as the following

$$R \equiv \frac{1}{N} \sum_{i=1}^N r_i r_i^\top \quad (1)$$

where N is the total number of atoms belonging to an aggregate and $r_i = (x_i, y_i, z_i)^\top$ is the position column vector of the i^{th} atom in the center of mass coordinate system (i.e. $\sum_{i=1}^N r_i = 0$). Following the description presented by Diful et al.¹ the radius of gyration tensor is diagonalized to obtain the principle moments of the gyration tensor. These are the eigenvalues $R_{1,2,3}$ which are then ordered such that $R_1 > R_2 > R_3$. The eigenvalues uniquely classify the shape of a given aggregate since $R_1 > R_2 \approx R_3$ is characteristic of a cylinder, $R_1 \approx R_2 \approx R_3$ is characteristic of a sphere, and $R_1 \approx R_2 > R_3$ is representative of a disk. Two ratios of the eigenvalues, $\gamma = (R_2/R_1)^2$ and $\zeta = (R_3/R_1)^2$ are utilized to effectively classify the shape of a given aggregate. If $\gamma \approx 1$ and $\zeta \approx 1$ the shape is close to spherical, while if both $\gamma \approx 0$ and $\zeta \approx 0$ the shape is close to cylindrical, and if $\gamma \approx 1$ and $\zeta \approx 0$ the shape is roughly a disk. This scheme is useful since it is represented visually as a 2D contour plot as and can quickly and easily describe a micellar system. A schematic is presented in Figure S10.

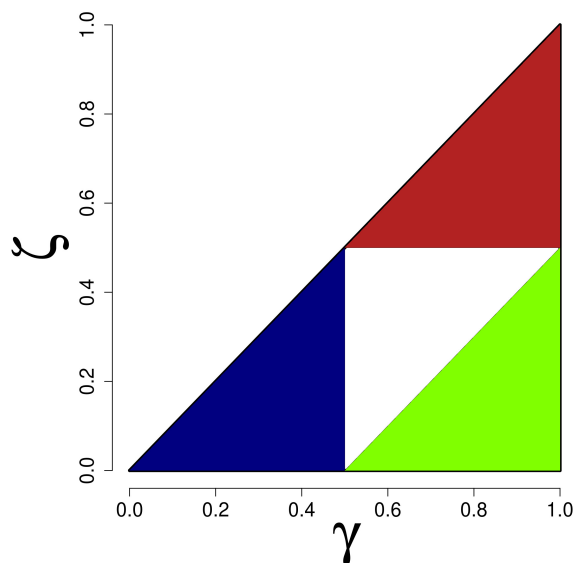


Figure S10. A schematic overview of the contour map used to classify aggregate shape. The three colored regions correspond to the three broad classes of shapes encountered in this work: red-spherical, blue-cylindrical, and green-disk. The white triangular region corresponds to an intermediate state. It should be noted that in practice no samples should exceed the bold black lines of the large triangle since both γ and ζ are the squares of the ratios of the principle moments, but that this is an artifact of kernel density estimation.

Figure 5 shows the results of the analysis of the radius of gyration for four representative aggregates, N11(D2), N48(D7), N52(D7), and N61(D27) where N is the number of Rha-C10-C10 molecules and D is the number of decane molecules. It is evident from the figure that as the overall size of the aggregate increases, the peak shifts towards the lower left of the contour map, which corresponds to a cylindrical shape. The smaller aggregate N11(D2) (**a**) briefly samples disk like conformations while the largest structure N61(D27) (**d**) is strictly cylindrical. It should be noted that no samples should exceed the triangular boundaries since both γ and ζ are the squares of the ratios of the principle moments, but that this is an artifact of kernel density estimation. The majority of the structures sampled were in the cylindrical region. Smaller, pre-micellar aggregates (total size < 20) are highly eccentric and sample larger regions of conformations.

References

- (1) Diful, A. G.; Avalos, J. B.; Mackie, A. D. Model Shape Transitions of Micelles: Spheres to Cylinders and Disks. *Langmuir* **2012**, 28, 3730–3743, PMID: 22292910.